2026 IEEE International Conference on Robotics and Automation (ICRA 2026)
June 1-5, 2026. Vienna, Austria

Efficient Frontier-Sampling-Mixed Autonomous Exploration Using Environmental Complexity

Liang Lu[1,2*], Ming Xiang[2*], Dongyang Tang[2], Zefeng Yan[2], Hao Wang[2] and Bin Han[2†], *Senior Member, IEEE*

***Abstract*— When exploring complex unknown environments, unmanned aerial vehicles (UAVs) often experience reduced efficiency and robustness due to unevenly distributed occlusions. This paper proposes an efficient hybrid autonomous exploration algorithm that adapts to environmental complexity, enabling effective frontier detection and viewpoint sampling to minimize overall exploration time. We introduce a frontier detection method based on a limited field of view (FOV), along with a unique ID-based frontier management mechanism, which ensures detection completeness while significantly reducing computational and memory overhead. Furthermore, an adaptive sampling strategy incorporating environmental complexity is introduced. By adaptively switching sampling modes and relaxing obstacle-free sphere generation constraints, the method improves both sampling efficiency and visibility evaluation performance. For path planning, a hierarchical planner based on a topological graph is constructed. It jointly optimizes global coverage paths and local frontier information to generate smooth and time-optimal trajectories. Both simulation and real-world experiments validate the advantages of the proposed approach in terms of exploration efficiency, computational overhead, and coverage rate.**

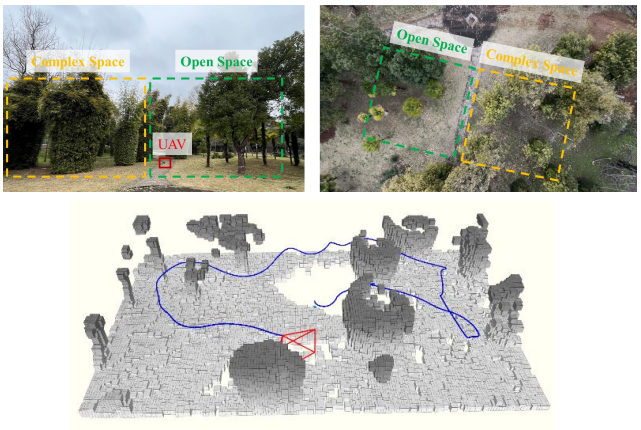

Fig. 1. Real-world outdoor exploration in a natural environment with irregular terrain and unevenly distributed obstacles. The quadrotor performs fully onboard real-time mapping and obstacle avoidance. Orange and green indicate complex and open areas, respectively.

I. INTRODUCTION

Autonomous exploration is essential for unmanned aerial vehicles (UAVs) to map and navigate in unknown environments, with applications in infrastructure inspection, search and rescue, and 3D reconstruction [1] [2]. However, due to limited onboard computing power and energy, achieving efficient exploration in complex settings remains challenging.

Environments with uneven occlusions, such as forests or ruins, often contain both open areas and dense obstacles. Many current methods prioritize regions with high volumetric gain, frequently neglecting obscured areas and resulting in repeated scans and inefficient paths. Existing approaches include sampling-based methods, which generate random viewpoints for guidance, offering flexibility but often converging to local optima, and frontier-based methods, which detect map boundaries (frontiers) to guide exploration, enabling global assessment but often producing inefficient back-and-forth movement. Recent hybrid approaches combine both strategies, yet often result in a loose coupling between local sampling and global frontier information, still failing to fully address redundant revisitation and global coordination.

To address these problems, we propose an efficient hybrid autonomous exploration algorithm that incorporates environmental complexity awareness. The main contributions are:

(1) A fast frontier detection method based on limited field-of-view (FOV) is proposed, which integrates historical FOV information to eliminate repeated detections. Combined with a unique ID-based frontier management mechanism, it achieves fast and complete detection within constrained regions.

(2) An adaptive fast viewpoint sampling is designed, which dynamically switches sampling modes according to environmental complexity. By relaxing the constraints for obstacle-free sphere generation instead of relying on computationally expensive ray casting, the method significantly improves sampling efficiency.

(3) A graph-based hierarchical planner is developed, which incrementally constructs an environmental topology graph to generate global coverage paths, locally optimizes the visitation sequence, and ultimately producing smooth, safe, and time-optimal trajectories.

This work was supported in part by the Jing-Jin-Ji Regional Integrated Environmental Improvement-National Science and Technology Major Project 2025ZD1206400, in part by the National Nature Science Foundation of China 52375015, and in part by the Interdiciplinary Research Program of HUST 2024JCYJ037.

[1] School of Artificial Intelligence and Automation, Huazhong University of Science and Technology, Wuhan 430074, China. [2] State Key Laboratory of Intelligent Manufacturing Equipment and Technology, School of Mechanical Science and Engineering, Huazhong University of Science and Technology, Wuhan 430074, China.

[*] These authors contributed equally to this work.

[†] Corresponding auther, binhan@hust.edu.cn

II. Related work

Autonomous exploration, a core capability for mobile robots to map unknown environments, has attracted sustained research attention. Existing approaches fall broadly into three categories: frontier-based, sampling-based, and hybrid methods.

Early work primarily centered on frontier-based methods. Yamauchi first introduced the concept of frontiers as boundaries between known and unknown regions [3]. These methods guide robots by detecting and moving toward frontiers to incrementally expand the mapped area. Subsequent studies improved efficiency and robustness. For instance, Keidar and Kaminka proposed the WFD and FFD algorithms, which enhance efficiency by restricting detection range and using sensor boundaries [4]. Quin et al. and Gao et al. introduced geometric optimization and cost modeling to reduce computational overhead [4] [5]. Stachniss et al. combined frontier exploration with a revisit mechanism to reduce SLAM uncertainty. As research advanced, these methods were extended to 3D scenarios [6]. Shen et al. employed stochastic differential equations to identify 3D frontiers [7]; Dornhege and Kleiner introduced the concept of empty cells for selecting highly visible viewpoints [8]; Zhu et al. implemented 3D frontier detection based on OctoMap [9]. While these methods enable global evaluation of candidate viewpoints, they often lead to inefficient back-and-forth movement.

In contrast, sampling-based methods typically generate candidate next-best views (NBVs) randomly in free space and evaluate their information gain. A notable example is NBVP by Bircher et al., which uses a receding horizon and RRT trees to generate viewpoints [10]. It performs well in isolated areas but is prone to local optima in complex environments. To mitigate this issue, Schmid et al. proposed an informative path planner based on large-scale single-trees [11], while Duberg maintained a graph structure to accelerate path queries [12]. Further studies introduced various improvements within the NBV framework. For instance, Papachristos et al. simultaneously optimized localization and mapping uncertainty in visually degraded environments [13]; Dang et al. employed salient voxels to guide exploration [14]; and Dharmadhikari et al. incorporated dynamic constraints into feasibility assessments [15]. However, these methods often employ greedy strategies, focusing on immediate information gain without global consideration, resulting in repeated visits and low exploration efficiency.

In recent years, researchers have attempted to develop hybrid methods that combine the strengths of both strategies. Selin et al. proposed Autonomous Exploration Planner (AEP), switching from local NBV to frontier guidance when stuck [16]; Dai et al. combined frontier extraction with local NBV sampling to evaluate candidates using a utility function [17]; Wang et al. efficiently computed information gain via incremental roadmap, but the completeness of frontier detection was challenging to guarantee [18]; Zhou et al. sampled local viewpoints around frontiers [19], while Yu et al. and Tang et al. improved viewpoint generation strategies to enhance efficiency [20] [21]; Cao et al. merged global subspace paths with local sampling, extending it to multi-robot systems [22]. Additionally, several studies attempted to incorporate coverage path for global guidance, but the high computational complexity of solving the TSP in 3D environments often makes it difficult to meet real-time requirements [23] [24].

In summary, while hybrid methods improve exploration performance, they still struggle to balance efficiency and real-time performance in complex environments. To address this, we propose an environment complexity-aware hybrid framework featuring fast frontier detection, adaptive sampling, and graph-based hierarchical planning for efficient and robust autonomous exploration on UAV platforms.

III. PROBLEM FORMULATION

This study addresses the problem of autonomous exploration by unmanned aerial vehicles (UAVs) in three-dimensional unknown environments. The environment is represented as a voxel map $\mathcal{M}$ (a 3D occupancy grid model, $V \subset \mathbb{R}^3$), which is partitioned into the following subspaces: unknown space V_{un} (unobserved regions), free space V_{free} (obstacle-free regions), and occupied space V_{occ} (obstacle regions). A free voxel is defined as a frontier voxel if it is adjacent to at least one unknown voxel. Connected frontier voxels form a frontier cluster $\mathcal{F}$. Specifically, a frontier voxel v_f (where $v_f \in V_{free}$ and adjacent to V_{un}) and the resulting frontier clusters $\mathcal{F}$ delineate the boundary between known and unknown regions.

The state of the UAV is defined as $x := p, \xi \in X \subset \mathbb{R}^4$, where $p = \{x, y, z\} \in \mathbb{R}^3$ denotes its position and $\xi \in \mathbb{R}$ represents the yaw angle. The map $\mathcal{M}$ is incrementally updated using depth sensor observations $O(x)$.

The exploration task is formulated as a trajectory optimization problem, with the objective of completely exploring the unknown space, that is, $V_{un} \to \emptyset$. At each planning cycle, a collision-free path γ entirely contained within V_{free} and satisfying all applicable constraints must be computed, such that it maximizes a utility function balancing information gain against motion cost:

$$\begin{aligned} \max_{\gamma} \quad & U(L(\gamma), I(\gamma)) \\ \text{s.t.} \quad & \gamma \subset V_{free}, \\ & g(\gamma) \geq 0. \end{aligned} \tag{1}$$

where $L(\gamma)$ denotes the motion cost along the path γ, $I(\gamma)$ represents the expected information gain along γ, that is, the anticipated volume of observable unknown space, and $g(\gamma) \geq 0$ incorporates kinematic and safety constraints.

IV. METHODOLOGY

This section details the environmental complexity-aware autonomous exploration framework for UAVs. The overall system architecture is shown in Fig. 2. The proposed method consists of three core modules: a limited field-of-view (FOV) based fast frontier detection and management mechanism, an adaptive viewpoint sampling strategy incorporating environmental complexity, and a hierarchical path planner built upon

a graph-based model. The overall pipeline commences with sensor-driven map updates, proceeds through frontier extraction and candidate viewpoint generation, performs global-to-local planning, and ultimately produces a smooth, safe, and time-optimal exploration trajectory.

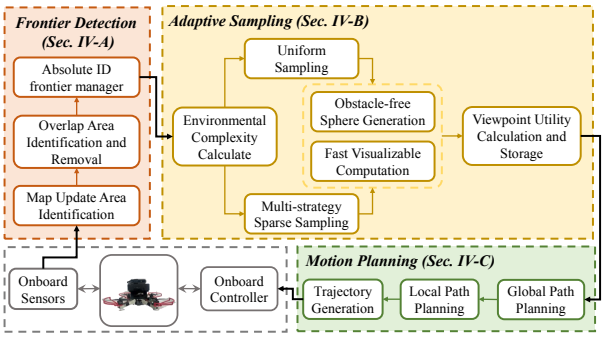

Fig. 2. Overall system architecture of the UAV autonomous exploration system.

A. Fast Frontier Detection and Unique ID Management

During exploration in unknown environments, particularly in areas with densely distributed occlusions, UAVs often exhibit back-and-forth movements, leading to heavily overlapping updated areas. To reduce redundancy while ensuring detection completeness, frontier detection is confined to incrementally updated areas. At each decision cycle, the system processes the current Axis-Aligned Bounding Box (AABB) $\mathcal{B}_t = [\mathbf{b}^t_{\min}, \mathbf{b}^t_{\max}]$, updated by sensor observations. The actual region to be processed is obtained by performing a differential operation between the current bounding box $\mathcal{B}_t$ and the previous one $\mathcal{B}_{t-1}$:

$$\mathcal{R}_t = \mathcal{B}_t \setminus (\mathcal{B}_t \cap \mathcal{B}_{t-1}) \tag{2}$$

This operation effectively avoids repeated processing and significantly reduces computational overhead. Meanwhile, the system maintains a global set of frontier clusters. A review mechanism is triggered for existing clusters that intersect both the updated and overlapping regions, preventing erroneous removal and ensuring the completeness of frontier detection, as depicted in Fig. 3.

Within the identified updated region $\mathcal{R}_t$, the algorithm performs connected-component growth to detect frontier voxels. To improve detection quality, the growth process introduces ground noise suppression and height-layer blocking constraints to align with the actual perceptual characteristics of the UAV. Subsequently, Principal Component Analysis (PCA) is used to segment and merge the generated frontier clusters, ensuring the rationality of cluster sizes.

To efficiently manage frontier cluster information, a unique ID is generated for each frontier cluster using a geometric encoding scheme:

$$\mathrm{ID} = H\left(\left\lfloor \frac{\bar{\mathbf{x}}_{\mathcal{F}}}{\delta} \right\rfloor, |\mathcal{F}|\right) \tag{3}$$

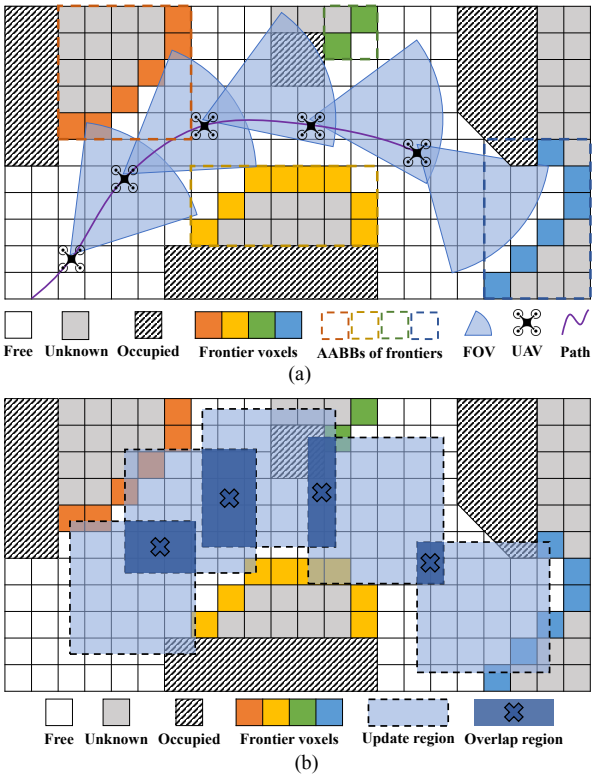

Fig. 3. Schematic diagram of historical overlap elimination in the updated region. (a) A UAV explores an unknown environment using its onboard camera; (b) Identification of current and historical updated regions from the FOV coverage area.

where $\bar{\mathbf{x}}_{\mathcal{F}}$ denotes the centroid coordinates of the frontier cluster, δ is the map resolution, $|\mathcal{F}|$ represents the size of the cluster, and $H(\cdot)$ is a hash function. This ID enables stable identification of the same cluster across planning cycles. Combined with a hash table data structure, it significantly reduces the computational cost associated with storing, retrieving, and updating cluster information. The resulting set of newly identified frontier clusters, denoted as $\widetilde{\mathcal{F}}$, serves as input to the subsequent sampling stage.

B. Adaptive Sampling Based on Environmental Complexity

1) Environmental Complexity Assessment: Environmental complexity $\mathcal{C}$ serves as a key indicator for guiding the sampling strategy, capturing both temporal variations of frontier evolution and spatial structural distribution. It is formulated as a weighted combination of the frontier change rate c_Δ and the spatial complexity c_s:

$$\mathcal{C} = w_\Delta c_\Delta + w_s c_s \tag{4}$$

The frontier change rate c_Δ reflects the dynamics of the exploration process. It is derived by normalizing the ratio of the number of newly detected frontier clusters between

consecutive cycles:

$$c_\Delta = \begin{cases} 0, & \text{if } |\tilde{\mathcal{F}}_{t-1}| = 0 \ \wedge \ |\tilde{\mathcal{F}}_t| = 0 \\ 1, & \text{if } |\tilde{\mathcal{F}}_{t-1}| = 0 \ \wedge \ |\tilde{\mathcal{F}}_t| > 0 \\ \frac{1}{2}\left[\tanh\big(2(\mathit{rate} - 1)\big) + 1\right], & \text{otherwise} \end{cases} \tag{5}$$

where $rate = |\tilde{\mathcal{F}}_t|/|\tilde{\mathcal{F}}_{t-1}|$, and $|\cdot|$ denotes the cardinality of the set, that is, the number of new frontier clusters.

The spatial complexity $\rfloor_s$ characterizes the spatial distribution characteristics of the frontier clusters and is composed of three normalized sub-metrics:

$$c_s = w_d f_d + w_{si} f_{si} + w_o f_o \tag{6}$$

In the above formulation, $f_d = \bar{d}/\widetilde{d}$ represents the distance dispersion, which is dimensionless. Here, $\bar{d}$ is the average pairwise distance between frontier clusters, reflecting their spatial spread. $\widetilde{d}$ is the ideal average pairwise distance derived from the chord length corresponding to the maximum FOV. This metric is inspired by the coefficient of variation in statistics. To better align with the sensor model and ideal exploration conditions, we replace the mean value in the original formula with a theoretical value derived from a scenario where the UAV equipped with a depth camera explores an open unknown environment. This theoretical value captures the expected spatial relationship between frontier clusters under ideal conditions, allowing f_d to express the deviation of the current average pairwise distance from the theoretical reference.

Similarly, $f_{si} = \sigma_{si}/\widetilde{\mu}_{sl}$ represents the scale dispersion, using a modified coefficient of variation to measure size variation among clusters. Here, $\widetilde{\mu}_{si}$ refers to the ideal average cluster size, which is obtained under maximum FOV visibility conditions.

The orientation dispersion, denoted as $f_o = \sigma_o/\widetilde{\mu}_o$ is computed by performing Principal Component Analysis (PCA) on each cluster in the $x-y$ plane to extract its principal direction. This metric quantifies the deviation in principal directions among clusters, thereby better reflecting the perception difficulty imposed by cluster orientations. In this expression, $\widetilde{\mu}_o$ represents the ideal average difference in principal directions, derived from the mean angular deviation of the clusters under maximum FOV conditions.

The overall complexity $\mathcal{C}$ determines the sampling mode: if $\mathcal{C}$ exceeds a predefined threshold, uniform sampling is adopted to ensure coverage; otherwise, polynomial sparse sampling is employed to achieve sufficient viewpoint distribution with lower computational cost.

2) Obstacle-Free Sphere Construction under Relaxed Conditions: To accelerate visibility evaluation, a maximum obstacle-free sphere ε is constructed for each frontier cluster $\widetilde{\mathcal{F}}$, centered at its average centroid $\bar{\mathbf{x}}_{\mathcal{F}}$. The initial sphere radius is defined as $r_0 = (1/2)s$, where $s = \max_{i,j}\|\mathbf{x}_i - \mathbf{x}_j\|$ denotes the cluster span. By incorporating the complexity measure $\mathcal{C}$, the construction conditions are relaxed: collision detection is performed along a limited set of directions with a step size of $2s_{cell}$, where s_{cell} is the map resolution. If no occupied voxel is detected, the sphere radius is expanded until $r \le r_{\max} = \max\left(\sqrt{2}\, r_0,\, r_{\max}^{(\mathrm{cfg})}\right)$, where $r_{max}^{(cfg)}$ is a predefined maximum expansion radius. The radius r must also satisfy the minimum enclosing requirement that covers a specified proportion of voxels in $\widetilde{\mathcal{F}}$. The final obstacle-free sphere is defined as:

$$\varepsilon = \mathbf{x} \in \mathbb{R}^3 : \| \mathbf{x} - \bar{\mathbf{x}}_{\mathcal{F}} \| \le r \tag{7}$$

The sphere ε is subsequently used to replace the computationally expensive full FOV ray casting. The sphere approximation is employed to estimate the number of detectable unknown voxels in the next exploration step, thereby further accelerating visibility evaluation process.

3) Candidate Viewpoint Generation and Fast Visibility Evaluation: Following the aforementioned complexity-aware strategy, uniform sampling is employed in complex regions, as indicated by the orange markers in Fig. 4 (left). These areas feature densely and irregularly distributed obstacles. In open regions, as shown by the green markers in Fig. 4 (right), polynomial sparse sampling is applied. Such regions are characterized by structural simplicity, sparse obstacles, uniform spatial distribution of frontier clusters, and high directional consistency, resulting in lower perception and exploration difficulty.

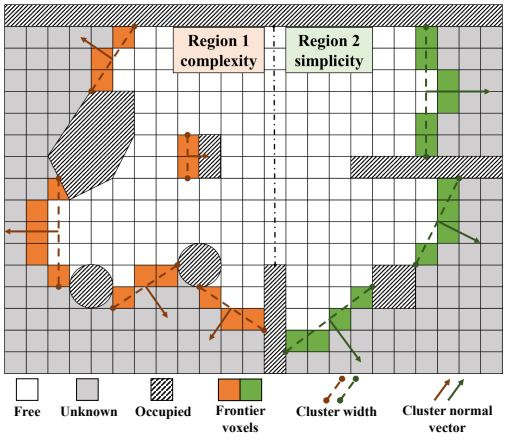

Fig. 4. Illustration of frontier distribution differences caused by varying obstacle densities in complex environments.

As indicated by the orange markers on the left side of Fig. 5, uniform sampling generates candidate viewpoints on the horizontal plane around the cluster centroid $\bar{\mathbf{x}}_{\mathcal{F}}$ by sampling multiple concentric circles with constant radial and angular steps:

$$r_k = r_{\min} + k\,\Delta r, \quad k = 0, \ldots, N_r - 1 \tag{8}$$

$$\Delta r = \frac{r_{\max} - r_{\min}}{N_r - 1} \tag{9}$$

$$\phi_m = \phi_0 + m\,\Delta\phi \tag{10}$$

$$\mathbf{p}_{k,m} = \bar{\mathbf{x}} + \begin{bmatrix} r_k \cos\phi_m \\ r_k \sin\phi_m \\ 0 \end{bmatrix} \tag{11}$$

The yaw angle $\psi_{k,m}$ of each candidate point is computed as the average direction of all voxels within $\widetilde{\mathcal{F}}$. Candidate points are further filtered according to the following constraints: they must lie within the map boundaries, belong to free space, maintain a minimum clearance from unknown or occupied regions, and keep a minimum distance from the current UAV position.

As shown by the green markers on the right side of Fig. 5, polynomial sparse sampling first projects the frontier cluster onto the horizontal plane and approximates its shape using a cubic polynomial via least squares method:

$$y = \sum_{j=0}^{3} a_j x^j \tag{12}$$

After sampling at equal intervals along the curve, each point is offset in the direction of the normal vector $\mathbf{n} = \frac{1}{\|\cdot\|}\left[-\sin\alpha,\ \cos\alpha\right]$ (where $\alpha = \arctan 2(dy/dx, 1)$) of the tangent vector $\mathbf{t} = [1, dy/dx]$ toward the free space. The points are then elevated to the average height of the cluster to form a set of 3D candidate viewpoints. The same filtering constraints as those applied in uniform sampling are enforced.

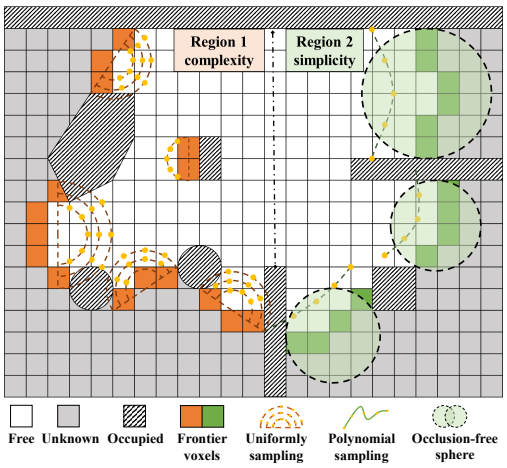

Fig. 5. Illustration of the hybrid sampling strategy incorporating environmental complexity.

Visibility evaluation is used to estimate the number of unknown voxels observable from a viewpoint, which serves as the information gain of the viewpoint (or its corresponding frontier cluster). To replace the high computational cost of conventional ray casting method, we introduce a fast approximation method based on obstacle-free spheres and propose a multi-stage evaluation mechanism to balance computational efficiency and visibility accuracy. Specifically, if the obstacle-free sphere $\mathcal{E}$ constructed at the centroid of the candidate cluster satisfies the following activation condition:

(i) Sufficient volume:

$$\mathrm{vol}(\mathcal{E}) \ \geq\ \tfrac{4}{3}\pi\left(\gamma\tfrac{s}{2}\right)^3, \quad \gamma \in (0,1) \tag{13}$$

(ii) Adequate proportion of candidate points within the sphere:

$$num\left(\mathbf{p}_{\mathcal{E}}\right) \geq \eta \times num\left(\mathbf{p}\right) \tag{14}$$

A balanced evaluation strategy is activated when only the volume constraint is satisfied. For viewpoints located within the sphere that possess visibility, it is unnecessary to perform full FOV ray casting. Instead, the information gain is approximated by counting unknown voxels within $\mathcal{E}$:

$$\widehat{N}_{\mathrm{unk}}(\mathbf{p}) \approx \sum_{v\in\mathcal{E}} \eta[v \in \mathcal{E} \wedge v = v_{un}] \cdot \mathrm{vol}(\mathcal{E}) \tag{15}$$

For the remaining viewpoints, conventional ray casting is still employed. This approach significantly reduces computational cost while preserving estimation accuracy. Finally, to avoid redundancy caused by excessively small differences in information gain among candidates, Z-score filtering is applied for selection. Let the set of gains for candidates from the same cluster be N_i, then compute:

$$z_i = \frac{N_i - \mu}{\sigma} \tag{16}$$

$$\mu = \frac{1}{K}\sum_i N_i \tag{17}$$

$$\sigma = \sqrt{\frac{1}{K}\sum_i (N_i - \mu)^2} \tag{18}$$

Only high-value candidate points satisfying $z_i \geq \kappa$ are retained. If σ is too small (indicating nearly equivalent gains among candidate points), all candidate points are retained directly. This layer reduces some computational redundancy while ensuring a certain level of accuracy. When none of the activation conditions are met, the original full ray casting method combined with the Z-score filtering mechanism is preserved as a robust fallback solution.

Through this hierarchical strategy, the algorithm adaptively switches evaluation methods under different conditions: it prioritizes fast yet approximate approaches when the environmental structure is relatively simple, and reverts to accurate though more computationally expensive conventional methods when constraints are insufficient. Thereby, it achieves an overall balance between computational efficiency and mapping completeness.

C. Hierarchical Path Planning Based on Topological Maps

1) Incremental Connectivity Topology Graph Construction: During exploration, to characterize the reachability and regional structural relationships of the environment, a topological graph $G = (V, E)$ is constructed. Here, vertices V represent the central points of regions with different occupancy states in the environment, while edges E represent the reachability relationships between regions. Formally, the graph is defined as:

$$G = (V_{free} \cup V_{un}, E_{free} \cup E_{un} \cup E_{portal}) \tag{19}$$

To enable online incremental construction, the environment is dynamically partitioned into several local regions after each map update, based on the occupancy state of the voxel map. The geometric centers of these regions are extracted as vertices. Subsequently, an edge is inserted between two regions if they are geometrically adjacent and connected through a navigable boundary. In this way, the topological graph continuously expands along with the exploration process, gradually delineating the hierarchical topological structure of the environment. This method avoids full global map reconstruction, and instead adopts a region-level abstract representation, thereby, decoupling the update overhead from environment scale. This ensures real-time performance and scalability in large-scale scenarios.

2) Hierarchical Planning and Decision-Making: Based on the incrementally constructed connectivity topology graph, a hierarchical path planning mechanism is proposed. By combining high-level graph search with low-level trajectory optimization, a balance between exploration efficiency and safety is achieved.

The high-level regional planning operates on the connectivity topology graph G. Predefined map grids are assigned, and the UAV's current position together with the optimal viewpoint of the frontier cluster in its current grid are inserted into G. To determine an exploration sequence that maximizes coverage of the remaining unknown regions, the problem is formulated as an instance of the Asymmetric Traveling Salesman Problem (ATSP). The edge weight between nodes is defined by a cost function that integrates the A* search distance d, obstacle density ρ, and an exploration risk factor r, capturing regional path efficiency and environmental difficulty. The resulting high-level planning cost is given by:

$$J_{high}(p) = \sum_{(u,v)\in p} \left(d(u,v) + \lambda_1 \rho(v) + \lambda_2 r(v)\right) \tag{20}$$

where λ_1 and λ_2 are weighting parameters. Edges returning to the starting node in G are assigned zero cost, indicating that the UAV is not required to return to its initial position. The optimal visiting sequence is obtained using an appropriate ATSP solver. During transitions between consecutive targets, a motion planner is invoked to generate dynamically feasible and smooth trajectories that satisfy the UAV's motion constraints. To achieve smoothness and dynamic feasibility, the low-level objective function is defined as:

$$J_{low} = \int_{t_0}^{t_f} \left(\| \dot{x}(t) \|^2 + \mu \| \ddot{x}(t) \|^2 \right) dt \tag{21}$$

where $\dot{x}(t)$ and $\ddot{x}(t)$ represent the velocity and acceleration respectively, and μ is the smoothness weight.

This hierarchical design effectively coordinates global exploration planning with local motion constraints, reducing computational complexity while maintaining planning quality. In unknown environments with unevenly distributed occlusions, the strategy also helps minimize inefficient exploratory motions caused by unguided behavior, enabling efficient and near-globally-optimal exploration of unknown spaces.

V. EXPERIMENTAL EVALUATION

A. Benchmark and Analysis

All simulation experiments are conducted on a computer equipped with an AMD R7-5800H CPU, a GeForce RTX 3060 6GB GPU, and 32 GB RAM. The algorithms are implemented on the ROS platform using C++. In the proposed framework, the Asymmetric Traveling Salesman Problem (ATSP) is solved using the LKH solver. The voxel resolution is set to 0.1 m, with a ground filtering height of 0.5 m. The maximum linear velocity, linear acceleration, and angular velocity are configured to 2 m/s, 3 m/s^2, and 1.57 rad/s, respectively. The sensor (FOV) is set 80° × 60°, with a perception range of 5 m. These parameters are selected based on typical UAV dynamics and sensor constraints to balance exploration efficiency and safety. Although varying these parameters may affect absolute exploration time, the relative performance comparisons between methods remain valid, as all baselines are evaluated under identical conditions. Replanning is triggered by three types of events: frontier updates, unsafe trajectory detection, and fixed time intervals for state machine updates.

To evaluate the proposed framework in simulation, we benchmarked it across three distinct environments: a Complex Office, Octa Maze, and a Real Forest, as illustrated in Fig. 6. These environments cover structured indoor, multi-layer occluded, and unstructured outdoor scenarios, providing representative conditions to evaluate generalizability. It is worth noting that the forest scene is constructed from a 3D point cloud map acquired using a hand-held LiDAR scanner. The benchmark experiments select a variety of exploration planners driven by visual perception in recent years as baselines. These methods generally prioritize the goal of quickly completing the exploration task, including Fuel [19] and Falcon [25]. Each method is executed three times under identical configurations in all tests. The statistical results and exploration trajectories of the three approaches are summarized in Table I and Fig. 7, respectively. Total exploration time is adopted as the primary metric, as it comprehensively reflects both path efficiency and decision-making overhead under identical dynamic constraints. The reported average and standard deviation indicate stable performance across repeated trials, demonstrating statistical consistency.

TABLE I
EXPLORATION STATISTICS IN THE COMPLEX OFFICE, OCTA MAZE, AND REAL FOREST SCENARIOS

Scene	Method	Frontier (ms)		Sampling (ms)		Exploring (s)
		Avg	Std	Avg	Std	Avg
Complex Office	Fuel [19]	3.54	1.49	4.69	3.46	319.10
	Falcon [25]	4.87	2.57	7.41	5.58	162.99
	Proposed	3.34	2.15	1.96	2.44	146.89
Octa Maze	Fuel [19]	3.43	1.56	6.33	4.79	421.28
	Falcon [25]	4.90	2.71	6.72	4.70	232.76
	Proposed	3.42	2.31	2.30	2.84	221.34
Real Forest	Fuel [19]	7.22	2.88	7.06	4.63	228.73
	Falcon [25]	13.17	6.82	10.99	6.01	126.66
	Proposed	8.68	5.36	4.27	3.49	117.74

(a) Complex Office (b) Octa Maze (c) Real Forest

Fig. 6. Simulation environments used for evaluation.

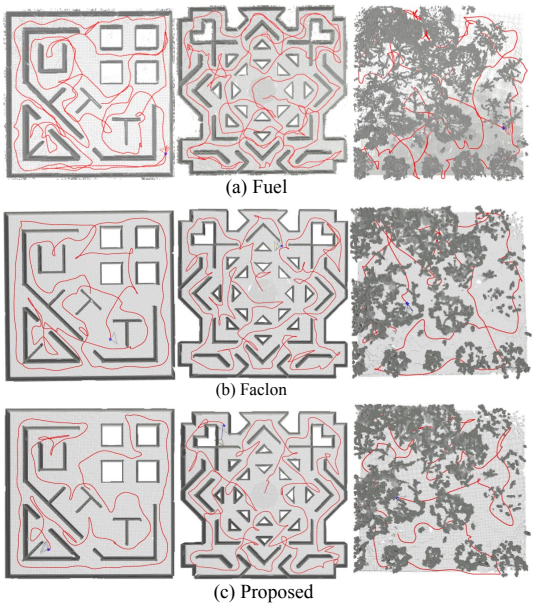

(a) Fuel

(b) Faclon

(c) Proposed

Fig. 7. Benchmarking results across all simulation environments.

1) Complex Office Scenario: In the classic Complex Office scenario, the proposed method demonstrates superior performance across multiple metrics compared to baseline algorithms. As shown in Fig. 8 (a), our method achieves faster coverage progression over time. The proposed approach maintains efficient frontier detection with an average time of 3.34 ms and standard deviation of 2.15 ms, outperforming both Fuel and Falcon. For viewpoint sampling, our method requires only 1.96 ms on average with a standard deviation of 2.44 ms, significantly better than Falcon (7.41 ms, 5.58 ms) and Fuel (4.69 ms, 3.46 ms). Most notably, the proposed method completes the exploration in 146.89 s, representing a 54% improvement over Fuel (319.10 s) and a 9.9% improvement over Falcon (162.99 s), while generating more efficient trajectories with reduced redundant visits.

2) Octa Maze Scenario: The Octa Maze scenario evaluates algorithm performance in complex multi-layer structures with heavy occlusions. The proposed method maintains low and stable computational overhead in this challenging environment. Our approach achieves an average frontier detection time of 3.42 ms with a standard deviation of 2.31 ms, superior to both comparison methods. For sampling efficiency, the proposed method demonstrates significantly better performance (2.30 ms, 2.84 ms) compared to Falcon (6.72 ms, 4.70 ms) and Fuel (6.33 ms, 4.79 ms). As illustrated in Fig. 8 (b), the total exploration time of 221.34 s represents a 47.5% improvement over Fuel (421.28 s) and a 4.9% improvement over Falcon (232.76 s), indicating that our method generates more efficient global paths with reduced backtracking in structurally complex environments.

3) Real Forest Scenario: The Real Forest scenario presents highly unstructured and uneven occlusion distributions, testing algorithm adaptability under challenging conditions. As shown in Fig. 8 (c), the proposed method achieves the best exploration time performance (117.74 s), representing a 48.5% improvement over Fuel (228.73 s) and a 7.0% improvement over Falcon (126.66 s). While the average frontier detection time (8.68 ms) is slightly higher than Fuel (7.22 ms), our method demonstrates superior sampling efficiency (4.27 ms, 3.49 ms) compared to both Falcon (10.99 ms, 6.01 ms) and Fuel (7.06 ms, 4.63 ms). The results confirm that our adaptive sampling strategy and environmental complexity assessment mechanism effectively handle the challenges of wild and unstructured environments while maintaining stable performance.

B. Field Exploration Tests

To further validate the proposed method, outdoor field experiments are conducted in a natural environment featuring irregular terrain and unevenly distributed obstacles. The outdoor environment introduces natural structural irregularities, sensing noise, and environmental uncertainty, enabling evaluation of the proposed framework under more realistic operating conditions. The tests are performed on a micro-quadrotor equipped with an Intel RealSense D435 camera and a NUC 11 (i5-1340P) onboard computer. Across all experiments, the maximum linear velocity and maximum linear acceleration are set to 0.6 m/s and 1.5 m/s² respectively. It is worth noting that no external devices are used during the real-world experiments, and all algorithms are executed entirely onboard.

A real-world exploration test is carried out in an outdoor area of approximately $17 \times 11 \times 3\ m^3$, containing natural obstacles such as vegetation, uneven ground, and scattered structural elements. As shown in Fig. 1, orange regions indicate structurally complex areas, while green regions represent relatively open spaces. The quadrotor performed 3D maneuvers to explore unknown areas while avoiding obstacles in real time.

Both simulation and real-world outdoor experiments consistently demonstrate the efficiency and effectiveness of the proposed method in environments with unevenly distributed occlusions. Additional experimental details are provided in the supplementary video.

VI. CONCLUSION

This study presents a hybrid autonomous exploration framework for unmanned aerial vehicles in complex unknown environments. The method enhances detection efficiency through fast frontier detection with limited field-of-view and absolute ID management. An environmental complexity index is introduced to achieve adaptive sampling, and a hierarchical trajectory planner based on topological

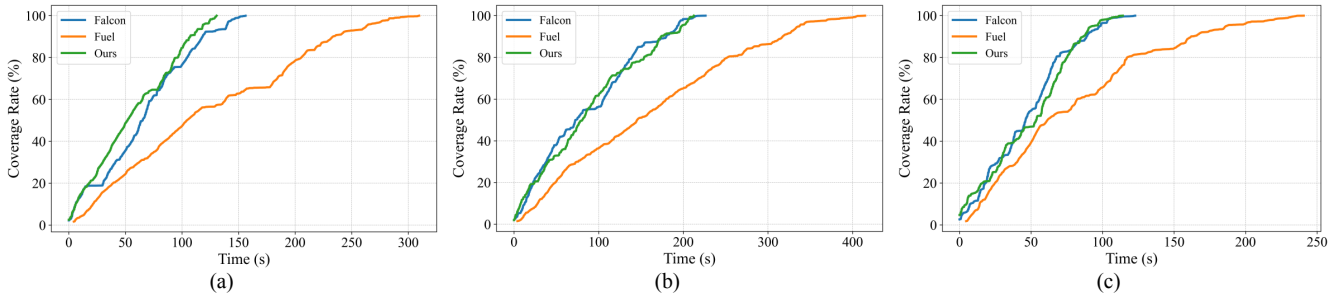

Fig. 8. Coverage comparison across different environments: (a) Complex Office, (b) Octa Maze, and (c) Real Forest.

graphs is combined to unify global coverage and local visitation, thereby generating smooth and efficient exploration trajectories.

Extensive simulations and real-world outdoor experiments demonstrate that the proposed method achieves superior exploration efficiency with reduced computational overhead, while maintaining real-time onboard performance. The results further verify the robustness and practical reliability of the framework in structurally diverse and realistic environments. Future work will incorporate dynamic obstacle modeling and predictive planning mechanisms to enhance adaptability in time-varying scenarios, as well as extend the framework to multi-UAV cooperative exploration.

REFERENCES

[1] B. Zhou, H. Xu, and S. Shen, "Racer: Rapid collaborative exploration with a decentralized multi-uav system," *IEEE Transactions on Robotics*, vol. 39, no. 3, pp. 1816–1835, 2023.

[2] C. Liang, X. Luo, X. Chen, and B. Han, "Route planning of truck and multi-drone rendezvous with available time window constraints of drones," *Science China Technological Sciences*, vol. 65, no. 9, pp. 2190–2204, 2022.

[3] M. Keidar and G. A. Kaminka, "Efficient frontier detection for robot exploration," *The International Journal of Robotics Research*, vol. 33, no. 2, pp. 215–236, 2014.

[4] P. Quin, D. D. K. Nguyen, T. L. Vu, A. Alempijevic, and G. Paul, "Approaches for efficiently detecting frontier cells in robotics exploration," *Frontiers in Robotics and AI*, vol. 8, p. 616470, 2021.

[5] W. Gao, M. Booker, A. Adiwahono, M. Yuan, J. Wang, and Y. W. Yun, "An improved frontier-based approach for autonomous exploration," in *2018 15th international conference on control, automation, robotics and vision (ICARCV)*. IEEE, 2018, pp. 292–297.

[6] C. Stachniss, D. Hahnel, and W. Burgard, "Exploration with active loop-closing for fastslam," in *2004 IEEE/RSJ International Conference on Intelligent Robots and Systems (IROS)(IEEE Cat. No. 04CH37566)*, vol. 2. IEEE, 2004, pp. 1505–1510.

[7] S. Shen, N. Michael, and V. Kumar, "Stochastic differential equation-based exploration algorithm for autonomous indoor 3d exploration with a micro-aerial vehicle," *The International Journal of Robotics Research*, vol. 31, no. 12, pp. 1431–1444, 2012.

[8] C. Dornhege and A. Kleiner, "A frontier-void-based approach for autonomous exploration in 3d," *Advanced Robotics*, vol. 27, no. 6, pp. 459–468, 2013.

[9] C. Zhu, R. Ding, M. Lin, and Y. Wu, "A 3d frontier-based exploration tool for mavs," in *2015 IEEE 27th International Conference on Tools with Artificial Intelligence (ICTAI)*. IEEE, 2015, pp. 348–352.

[10] A. Bircher, M. Kamel, K. Alexis, H. Oleynikova, and R. Siegwart, "Receding horizon path planning for 3d exploration and surface inspection," *Autonomous Robots*, vol. 42, no. 2, pp. 291–306, 2018.

[11] L. Schmid, M. Pantic, R. Khanna, L. Ott, R. Siegwart, and J. Nieto, "An efficient sampling-based method for online informative path planning in unknown environments," *IEEE Robotics and Automation Letters*, vol. 5, no. 2, pp. 1500–1507, 2020.

[12] D. Duberg and P. Jensfelt, "Ufoexplorer: Fast and scalable sampling-based exploration with a graph-based planning structure," *IEEE Robotics and Automation Letters*, vol. 7, no. 2, pp. 2487–2494, 2022.

[13] C. Papachristos, S. Khattak, and K. Alexis, "Uncertainty-aware receding horizon exploration and mapping using aerial robots," in *2017 IEEE international conference on robotics and automation (ICRA)*. IEEE, 2017, pp. 4568–4575.

[14] T. Dang, C. Papachristos, and K. Alexis, "Visual saliency-aware receding horizon autonomous exploration with application to aerial robotics," in *2018 IEEE international conference on robotics and automation (ICRA)*. IEEE, 2018, pp. 2526–2533.

[15] M. Dharmadhikari, T. Dang, L. Solanka, J. Loje, H. Nguyen, N. Khedekar, and K. Alexis, "Motion primitives-based path planning for fast and agile exploration using aerial robots," in *2020 IEEE International Conference on Robotics and Automation (ICRA)*. IEEE, 2020, pp. 179–185.

[16] M. Selin, M. Tiger, D. Duberg, F. Heintz, and P. Jensfelt, "Efficient autonomous exploration planning of large-scale 3-d environments," *IEEE Robotics and Automation Letters*, vol. 4, no. 2, pp. 1699–1706, 2019.

[17] A. Dai, S. Papatheodorou, N. Funk, D. Tzoumanikas, and S. Leutenegger, "Fast frontier-based information-driven autonomous exploration with an mav," in *2020 IEEE international conference on robotics and automation (ICRA)*. IEEE, 2020, pp. 9570–9576.

[18] C. Wang, H. Ma, W. Chen, L. Liu, and M. Q.-H. Meng, "Efficient autonomous exploration with incrementally built topological map in 3-d environments," *IEEE Transactions on Instrumentation and Measurement*, vol. 69, no. 12, pp. 9853–9865, 2020.

[19] B. Zhou, Y. Zhang, X. Chen, and S. Shen, "Fuel: Fast uav exploration using incremental frontier structure and hierarchical planning," *IEEE Robotics and Automation Letters*, vol. 6, no. 2, pp. 779–786, 2021.

[20] J. Yu, H. Shen, J. Xu, and T. Zhang, "Echo: An efficient heuristic viewpoint determination method on frontier-based autonomous exploration for quadrotors," *IEEE Robotics and Automation Letters*, vol. 8, no. 8, pp. 5047–5054, 2023.

[21] B. Tang, Y. Ren, F. Zhu, R. He, S. Liang, F. Kong, and F. Zhang, "Bubble explorer: Fast uav exploration in large-scale and cluttered 3d-environments using occlusion-free spheres," in *2023 IEEE/RSJ International Conference on Intelligent Robots and Systems (IROS)*. IEEE, 2023, pp. 1118–1125.

[22] C. Cao, H. Zhu, H. Choset, and J. Zhang, "Exploring large and complex environments fast and efficiently," in *2021 IEEE international conference on robotics and automation (ICRA)*. IEEE, 2021, pp. 7781–7787.

[23] L. Lu, X. Gao, H. Wang, M. Xiang, Z. Zhang, and B. Han, "Distributed task planning method for synchronous execution of heterogeneous tasks in uncertain environments," *IEEE Transactions on Automation Science and Engineering*, pp. 1–1, 2026.

[24] X. Kan, H. Teng, and K. Karydis, "Online exploration and coverage planning in unknown obstacle-cluttered environments," *IEEE Robotics and Automation Letters*, vol. 5, no. 4, pp. 5969–5976, 2020.

[25] Y. Zhang, X. Chen, C. Feng, B. Zhou, and S. Shen, "Falcon: Fast autonomous aerial exploration using coverage path guidance," *IEEE Transactions on Robotics*, 2024.